



# Three electrodes analysis of a 3 V-class all-solid-state lithium-ion battery based on garnet-type solid electrolyte $\text{Li}_{6.4}\text{La}_3\text{Zr}_{1.4}\text{Ta}_{0.6}\text{O}_{12}$

Yue Jiang<sup>a</sup>, Xiaohong Zhu<sup>a,\*</sup>, Wei Lai<sup>b,\*\*</sup>

<sup>a</sup> College of Materials Science and Engineering, Sichuan University, Chengdu, 610064, China

<sup>b</sup> Department of Chemical Engineering and Materials Science, Michigan State University, East Lansing, MI, 48824, USA

## HIGHLIGHTS

- $\text{Li}_2\text{CO}_3$  is used to mitigate high-temperature side reactions in LNM|LLZT|LTO.
- The voltage of such an all-solid-state battery reaches beyond 3 V.
- Three-electrode configuration separates the contributions of electrodes and electrolyte.

## ARTICLE INFO

### Keywords:

All-solid-state lithium-ion battery  
Garnet-type electrolyte  
LNM  
LTO  
Three-electrode configuration

## ABSTRACT

At present, fabrication of all-solid-state lithium-ion batteries using garnet-type electrolytes is still challenging due to issues with interfacial stability and interfacial impedance caused by the high-temperature sintering process. In this work, we employ  $\text{Li}_2\text{CO}_3$  as additive to mitigate high-temperature side reactions and prepare an all-solid-state battery LNM|LLZT|LTO using spinel-structured  $\text{LiNi}_{0.5}\text{Mn}_{1.5}\text{O}_4$  (LNM) and  $\text{Li}_4\text{Ti}_5\text{O}_{12}$  (LTO) as electrodes and garnet-type  $\text{Li}_{6.4}\text{La}_3\text{Zr}_{1.4}\text{Ta}_{0.6}\text{O}_{12}$  (LLZT) as the electrolyte. The battery voltage reaches beyond 3 V and can be charged and discharged for 5 cycles at a rate of C/10. The three-electrode setup of the battery allows the separation of positive and negative electrodes in their voltage profiles and impedance responses during cycling. Our results suggest that the high-voltage electrode LNM can work with LLZT in a solid-state-battery configuration and the negative electrode is the performance-limiting component.

## 1. Introduction

The conventional Li-ion batteries face safety issues such as the inherent risks of leakage, fire, or explosion, which are caused by the flammable organic liquid electrolytes [1]. When these electrolytes are combined with high voltage positive-electrodes, such as  $\text{LiNi}_{0.5}\text{Mn}_{1.5}\text{O}_4$  [2] and  $\text{LiNiPO}_4$  [3], it would lead to organic electrolyte decomposition. All-solid-state lithium-ion batteries using inorganic solid electrolytes have therefore been considered possible candidates to solve these problems as well as to offer a higher power and energy density [4]. Owing to its high conductivity ( $2.06 \text{ mS cm}^{-1}$  at room temperature) [5] and wide electrochemical window ( $\sim 6 \text{ V}$ ) [6,7], especially the excellent electrochemical performance with lithium-based positive-electrodes and even Li metal negative-electrode by a nano buffer layer [8,9], the garnet-type solid state electrolyte  $\text{Li}_7\text{La}_3\text{Zr}_2\text{O}_{12}$  (LLZ) is considered as

one of the most promising candidates to replace the organic or polymer electrolyte in Li-ion batteries.

At present, many works on all-solid-state lithium-ion batteries with garnet-type solid electrolyte LLZ mainly have been focused on using different methods to prepare different positive-electrodes on the surface of LLZ ceramic pellets directly, like pulse-laser-deposition PLD [10] or co-sintering with low-melting-point  $\text{Li}_3\text{BO}_3$  [11] to make positive-electrode|electrolyte double layer or with buffer layer in the middle [12,13] and then using Li metal on another side with or without buffer layer [14,15]. Although Li metal in rechargeable lithium-ion battery possesses the highest specific capacity ( $3860 \text{ mAh g}^{-1}$ ) and the lowest electrochemical potential ( $-3.04 \text{ V}$  vs. the standard hydrogen electrode) [16], it poses a severe safety issue. There are several experimental results showing that Li metal cannot be in direct contact with LLZ pellets, although it was considered that LLZ could be stable with Li metal

\* Corresponding author.

\*\* Corresponding author.

E-mail addresses: [xhzhu@scu.edu.cn](mailto:xhzhu@scu.edu.cn) (X. Zhu), [laiwei@msu.edu](mailto:laiwei@msu.edu) (W. Lai).

<https://doi.org/10.1016/j.jpowsour.2022.231278>

Received 1 September 2021; Received in revised form 21 February 2022; Accepted 6 March 2022

Available online 11 March 2022

0378-7753/© 2022 Elsevier B.V. All rights reserved.

when first reported by Murugan et al. [17]. For instance, about 6 nm thick tetragonal-like interface was formed in Al-doped cubic phase [18]; even 130  $\mu\text{m}$  thick tetragonal interface was formed in contact with Fe-doped cubic phase LLZ through the reduction of  $\text{Fe}^{3+}$  [19]. Since conductivity of tetragonal LLZ was two orders of magnitude lower than that of the high conductive cubic phase, this caused a huge interfacial impedance increase [20]. In addition, previous results showed that the direct contact of doped LLZ with Li metal for long duration led to redox reaction of constituent elements in LLZ, e.g.  $\text{Nb}^{5+}$  to  $\text{Nb}^{4+}$  in the  $\text{Nb}^{5+}$ -doped LLZ [21]. In addition, other results [22,23] showed that voids were formed at the Li/LLZ interface during cycles due to repeated Li deposition and dissolution. Hence, using Li metal in all-solid-state lithium-ion batteries based on garnet-type solid electrolyte LLZ is still challenging.

The flat potential of about 1.5 V versus  $\text{Li}^+/\text{Li}$  and near-zero structural change upon the insertion or extraction of  $\text{Li}^+$  makes  $\text{Li}_4\text{Ti}_5\text{O}_{12}$  (LTO) spinel a promising lithium negative-electrode [24]. The application of LTO negative-electrode on garnet-type solid electrolyte to prepare half cells was performed by SPS method [25], PLD method [26] and dropping LTO sol into a nano porous structure of pellet surface with heat treatment [27] to obtain a good interface with garnet-type LLZ, where Li metal was combined to prepare all-solid-state lithium battery. For example, Jin et al. [20] used PLD to make a  $\text{LiMn}_2\text{O}_4$ /solid electrolyte/LTO full cell with Al-doped LLZ pellet. Likewise, several works reported the use of LTO to prepare the full cell with the help of polymer electrolyte, such as  $\text{LiFePO}_4$ /solid electrolyte/LTO [28],  $\text{LiMn}_{0.8}\text{Fe}_{0.2}\text{PO}_4$ /solid electrolyte/LTO [29,30].

As a nickel-substituted product of  $\text{LiMn}_2\text{O}_4$ , the high-voltage spinel-structured  $\text{LiNi}_{0.5}\text{Mn}_{1.5}\text{O}_4$  (LNM) has drawn much attention for its electrochemical capability, a high voltage working platform (4.7 V vs.  $\text{Li}/\text{Li}^+$ ) and the great improvement in high temperature cycles [31,32]. There was an unsuccessful application of LNM along with Ga-doped LLZ that failed when reaching 3.8 V (vs Li) due to the reaction between LNM and electrolyte [33].

In this work, we report an all-solid-state Li-ion battery using LNM and LTO spinels as the active positive and negative electrode material, respectively. Both LNM and LTO will react with LLZ under co-sintering at high temperatures, producing non-Li-conducting  $\text{La}_2\text{Zr}_2\text{O}_7$  and large interfacial impedance. Very recently Yang et al. [34] added surplus  $\text{Li}_2\text{O}$  in the co-sintered  $\text{LiCoO}_2$  and  $\text{Li}_{6.4}\text{La}_3\text{Zr}_{1.4}\text{Ta}_{0.6}\text{O}_{12}$  at 600  $^\circ\text{C}$  for 5 h in the air to mitigate this effect. Researchers used the lower-melting-point lithium salt (e.g.  $\text{Li}_3\text{BO}_3$  with a melting point of 800  $^\circ\text{C}$ ) to improve the connection [35] and minimize the element cross-diffusion [36]; the silver powder was also added to improve the electronic conductivity as well as reduce the interface impedance [25] to prepare all-solid-state lithium batteries. Motivated by these reports, we carried out the preparation of LNM|LLZ|LTO battery at 800  $^\circ\text{C}$ , with the help of low-melting lithium salt  $\text{Li}_2\text{CO}_3$  (723  $^\circ\text{C}$ ) to mitigate Lithium loss, of  $\text{Li}_3\text{BO}_3$  to improve sintering, and of silver powders to enhance the electronic conductivity. As our objective was not to prepare a high-performance all-solid-state-battery, we utilized a cell with thick components and did not emphasize the optimization of materials compositions or processing conditions. Instead, we employed a three-electrode setup to characterize this tri-layer cell such that the charging/discharging voltage profiles and impedance responses of positive and negative electrodes, as well as electrolyte, could be separated. We hope information supplied by this separation could provide insights on how to improve individual components.

## 2. Experimental

Stoichiometric quantities of  $\text{LiOH}\cdot\text{H}_2\text{O}$  (Alfa Aesar, 98%),  $\text{La}_2\text{O}_3$  (Alfa Aesar, 99.9%),  $\text{ZrO}_2$  (Alfa Aesar, 99.7%) and  $\text{Ta}_2\text{O}_5$  (Alfa Aesar, 99.85%) were used as raw materials corresponding to the nominal compositions of  $\text{Li}_{6.4}\text{La}_3\text{Zr}_{1.4}\text{Ta}_{0.6}\text{O}_{12}$  (LLZT).  $\text{La}_2\text{O}_3$  powders were dried at 900  $^\circ\text{C}$  overnight in a MgO crucible. An excess of 10 wt%  $\text{LiOH}\cdot\text{H}_2\text{O}$

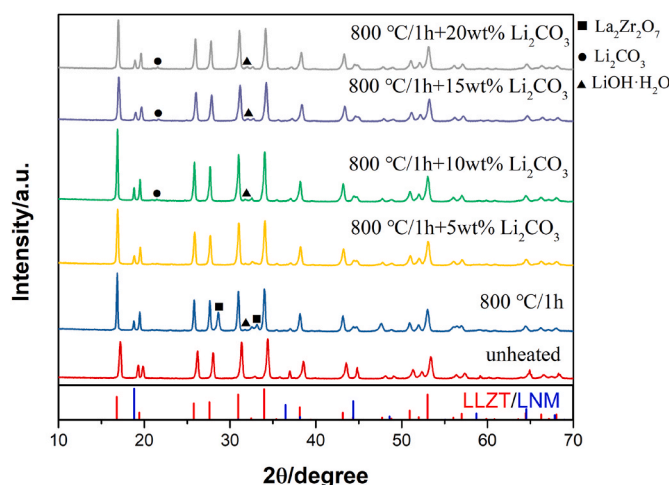


Fig. 1. Powder XRD patterns of LNM/LLZT mixture for different additive and heat treatment conditions.

was used to compensate for Li loss during the synthesis. Raw powders were wet-milled on a roller mixer overnight in a polyethylene jar filled with 2-propanol. After that, the mixed slurry was heated by IR heating in a MgO crucible, which were covered by a MgO lid. Then the homogeneously mixed powders were calcined at 1000  $^\circ\text{C}$  for 12 h with 2  $^\circ\text{C min}^{-1}$  heating rate and cooling rate. Afterwards, the obtained pure cubic phase LLZT (Fig. 1(s) in the supplemental materials) was mixed with spinel-structured electrodes  $\text{LiNi}_{0.5}\text{Mn}_{1.5}\text{O}_4$  (LNM, Fig. 2(s)) and  $\text{Li}_4\text{Ti}_5\text{O}_{12}$  (LTO, Fig. 3(s)) at 6:1 wt ratio, defined as positive-electrode and negative-electrode mixture, respectively. Both LNM and LTO were from MTI Corporation.  $\text{Li}_3\text{BO}_3$  (LBO) was prepared by vibrating mill of a mixture of  $\text{LiOH}\cdot\text{H}_2\text{O}$  and  $\text{H}_3\text{BO}_3$  (Alfa Aesar, 98%) based on the stoichiometric ratio, and subsequent sintering at 500  $^\circ\text{C}$  for 1 h and 600  $^\circ\text{C}$  for 2 h [37].

The positive-electrode mixture included LLZT (30 mg), LNM (5 mg),  $\text{Li}_2\text{CO}_3$  (Alfa Aesar, 99.985%, 1.75 mg), LBO (7 mg), and Ag (Sigma-Aldrich, 2–3.5  $\mu\text{m}$  in diameter, 99.9%, 35 mg).  $\text{Li}_2\text{CO}_3$  was added to mitigate the reaction between LLZT and LNM, while LBO acted as a sintering aid. Ag powder was used to improve the electronic conductivity. The negative-electrode mixture had 5 mg of LTO and 3.5 mg of  $\text{Li}_2\text{CO}_3$ , keeping the other compositions the same. The electrolyte layer had 1.2 g of LLZT and 0.24 g of LBO. Finally, the tri-layer samples were prepared with layer-by-layer pressing in a 10 mm diameter die under a uniaxial pressure of 120 MPa and then sintered at 800  $^\circ\text{C}$  for 1 h with 5  $^\circ\text{C min}^{-1}$  heating rate and cooling rate. The silver pastes were applied on both sides of the cell and then heated at 700  $^\circ\text{C}$  for 1 h as the counter collector.

In the three-electrode setup, silver pastes and wires were applied to the positive-electrode (working-electrode or we), electrolyte (reference-electrode or re), and negative-electrode (counter-electrode or ce) and sintered at 300  $^\circ\text{C}$  for 1 h to improve the connection. Cell tests were performed using the same setup combining a tube furnace and an electrochemical workstation (Bio-Logic SP-300) in our previous works [38] with air flow at 150  $^\circ\text{C}$ . A sinusoidal voltage signal with amplitude of 100 mV was applied for the frequency range of 200 kHz to 1 Hz in all-solid-state batteries and 3 MHz to 1 Hz in the electrolyte cell. The current on charging and discharging was set as 88.9  $\mu\text{A cm}^{-2}$  (0.1 C). The charging time was set as 10 h and discharging cut-off voltage of Ewe-ce was set at 0 V. At the end of charging/discharging, the cell was allowed to rest for 30 min before taking impedance measurement.

Powder X-ray diffraction was performed using the Bruker D2 ADVANCE diffractometer operating at 30 kV and 10 mA. The 2 $\theta$  measurement range was selected as 10–70 $^\circ$  with a step interval of 0.02 $^\circ$ . The morphologies and EDS mapping were measured by using field emission-

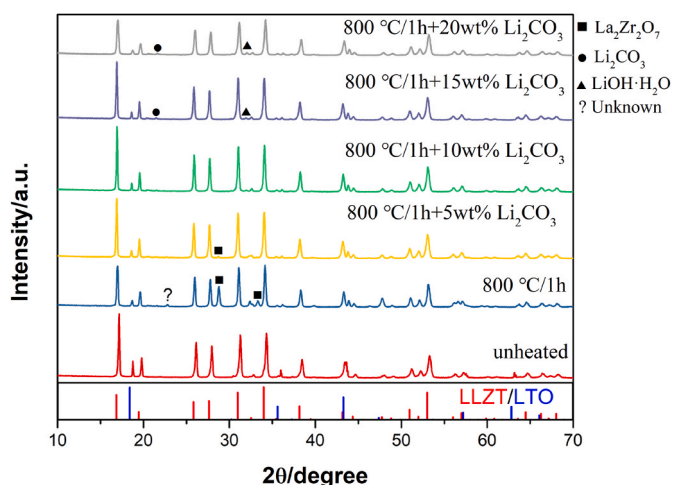


Fig. 2. Powder XRD patterns of LTO/LLZT mixture for different additive and heat treatment conditions.

scanning electron microscopy (FE-SEM, JSM-7500, Japan). XPS measurements were performed using Thermo ESCALAB 250XI with a monochromated AlK $\alpha$  X-ray source to find out the oxidation states of silver.

### 3. Results and discussion

Fig. 1 and Fig. 2 show the powder XRD patterns for different weight ratios of Li<sub>2</sub>CO<sub>3</sub> mixed with positive-electrode (LNM/LLZT) and negative-electrode (LTO/LLZT) mixture heated at 800 °C for 1 h, respectively. Without Li<sub>2</sub>CO<sub>3</sub>, mixtures would form a large amount of La<sub>2</sub>Zr<sub>2</sub>O<sub>7</sub> impurity after being heated at 800 °C compared to the unheated mixtures, revealing the lithium element loss during co-heating process. A similar result was reported by Miara et al. [39], where a significant reaction happened in LNM when mixed with the same volume of LLZT at a lower temperature of 600 °C. Hence, we use different amounts of Li<sub>2</sub>CO<sub>3</sub> mixed with positive-electrode and negative-electrode to compensate for lithium loss during the high temperature heating

process. Interestingly, with only 5 wt% Li<sub>2</sub>CO<sub>3</sub> addition, the impurity peak of La<sub>2</sub>Zr<sub>2</sub>O<sub>7</sub> in the positive-electrode mixture disappeared. With the same 5 wt% Li<sub>2</sub>CO<sub>3</sub> addition in the negative-electrode mixture (Fig. 2), only a slight amount of La<sub>2</sub>Zr<sub>2</sub>O<sub>7</sub> impurity was observed; impurity disappeared with 10 wt% Li<sub>2</sub>CO<sub>3</sub> addition. Some unknown phase (s) still existed in both positive and negative-electrode mixture even when the amount of Li<sub>2</sub>CO<sub>3</sub> was increased to 20 wt%. The reaction can also be inferred by the observation that the peak intensities of LNM and LTO were lower than those of the unheated samples, as reported previously [39].

After determining the optimal amount of Li<sub>2</sub>CO<sub>3</sub> addition (5% for positive-electrode and 10% for negative-electrode), we pressed the positive-electrode, electrolyte, and negative-electrode layer by layer and then heated the whole structure at 800 °C for 1 h. Fig. 3(a) shows the schematic configuration of the tri-layer-structured cell in this work. We used the same amount of silver powder (to enhance electronic conductivity) and Li<sub>3</sub>BO<sub>3</sub> (to enhance adhesion) in both the positive and negative-electrode mixtures. In order to probe the influence of Ag on electrodes, we used XPS spectra of Ag 3d to investigate the chemical state of Ag in those two mixtures, shown in Fig. 4(s). The two 3d peaks are 368.13/374.13 and 368.16/374.16 eV in the positive and negative electrodes, respectively. The splitting distance of the 3d doublet in two samples is 6.0 eV and thus corresponds to Ag<sup>0</sup> oxidation state [40], indicating that Ag exists as a metallic state in two mixtures. We added LLZT and 20 wt% of Li<sub>3</sub>BO<sub>3</sub> in the electrolyte layer.

SEM images and elemental distributions of portions of the cell are presented in Fig. 3(b) and (c). We can observe the good positive|electrolyte|negative interface. The signals of Mn, Ti, Ag indicated they were only in the electrode but not the electrolyte layer. Due to the small amount of Ni, it is hard to make conclusions on its distribution. We presented in Fig. 3(d) and (e) the element distribution across the interfaces of positive|electrolyte and negative|electrolyte by EDS line scan. Results indicated that Mn, Ni, Ti, Ag elements only existed in the electrode layers.

We carried out the electrochemical characterization of the cell using a three-electrode configuration (Fig. 4) where the working-electrode (we) and counter-electrode (ce) are positive and negative electrodes, respectively. The reference-electrode is silver. In this three-electrode

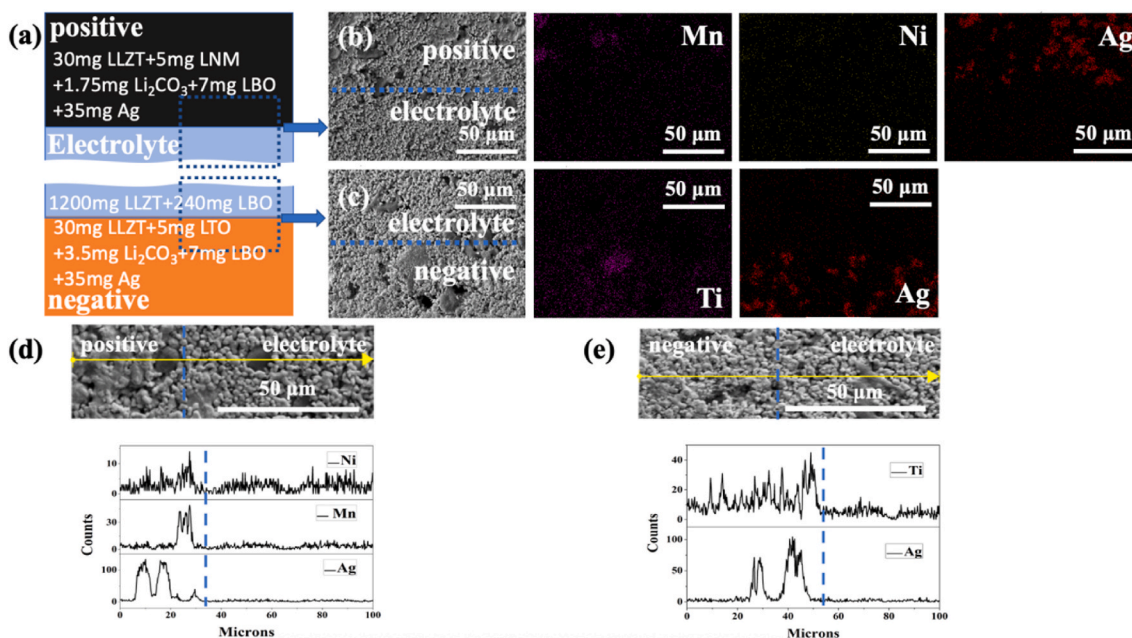


Fig. 3. (a) Schematic of tri-layer cell in this work. (b) Cross-section SEM image of positive-electrode (up) and electrolyte layer (down). EDS elemental mapping images of Mn, Ni and Ag. (c) Cross-section SEM image of electrolyte (up) and negative-electrode layer (down). EDS elemental mapping images of Ti and Ag. EDS lines profiles of (d) LNM/LLZT and (e) LTO/LLZT interface.

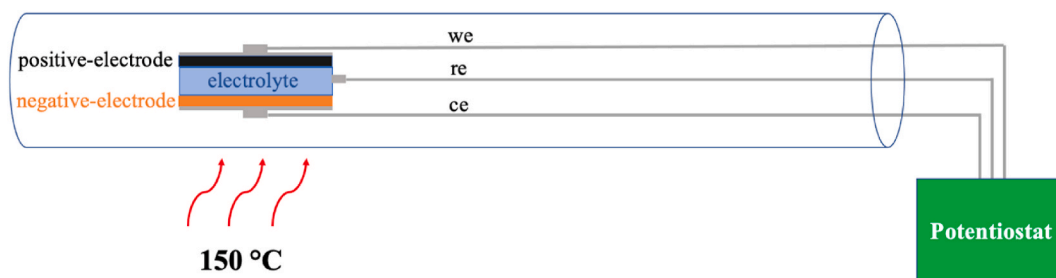


Fig. 4. Schematic of three-electrode testing configuration used in this work. (we: working-electrode; re: reference-electrode; ce: counter-electrode.)

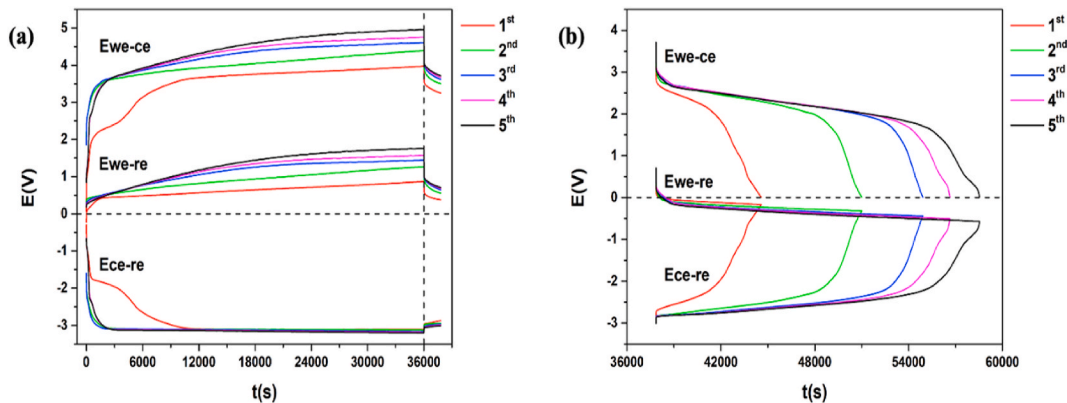


Fig. 5. (a) Charging and (b) discharging profiles (cut-off voltage of Ewe-ce was set at 0 V) of tri-layer sample using three-electrode method, tested at 150 °C under 0.1 C ( $88.9 \mu\text{A cm}^{-2}$ ) current.

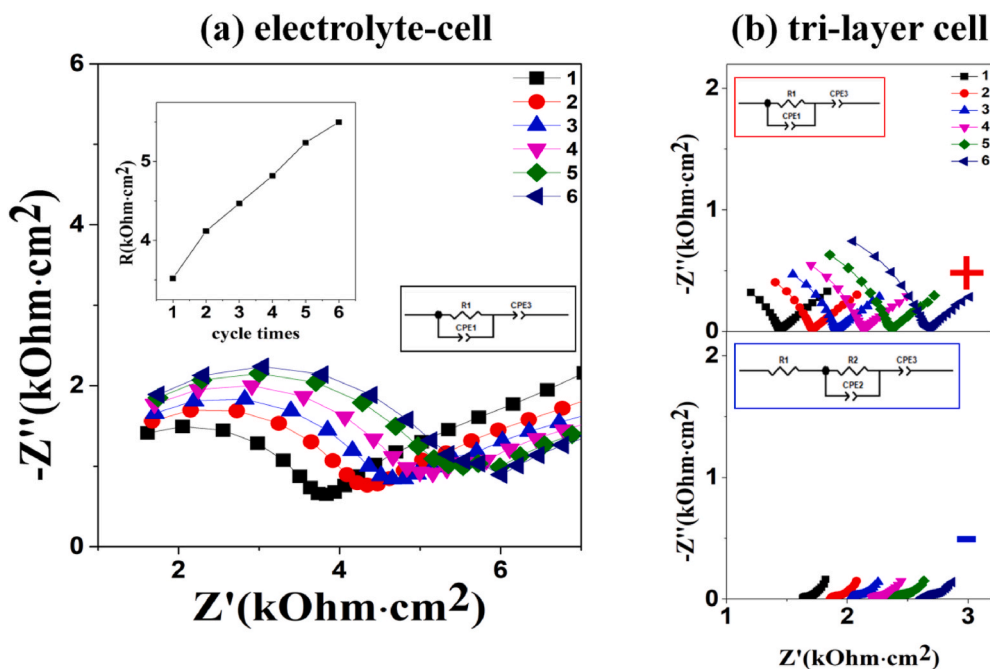


Fig. 6. Impedance spectra during the shelf tests (a) electrolyte-cell and (b) tri-layer cell tested every 10 h at 150 °C (air).

configuration, the contribution from the positive (as we-re) and negative (ce-re) can be separately measured. The whole cell signal is denoted as we-ce. Fig. 5(a) and Fig. 5(b) present the charging and discharging results of the tri-layer-structured cell under 0.1 C current at 150 °C for 5 cycles. While the charging behavior of positive-electrode, i.e. we-re, is typical of a sloping profile, the voltage change of negative-electrode starts with sharp decrease before turning into a “plateau”, a signature

behavior of LTO. From Fig. 5(a), the resting (after 30 min) voltage of Ece-re after the 10 h charging decreased slightly with cycling, while the voltage of Ewe-re increased significantly, leading to increased values of whole-cell voltage or Ewe-ce. These values are around 3.5 V, which is very close to the expected value of  $\sim 3.2$  V for LNM/electrolyte/LTO full cell, considering the flat operating voltage plateaus of  $\sim 4.7$  V in LNM and  $\sim 1.5$  V in LTO, respectively [41]. In the results of Hänsel et al. [33],

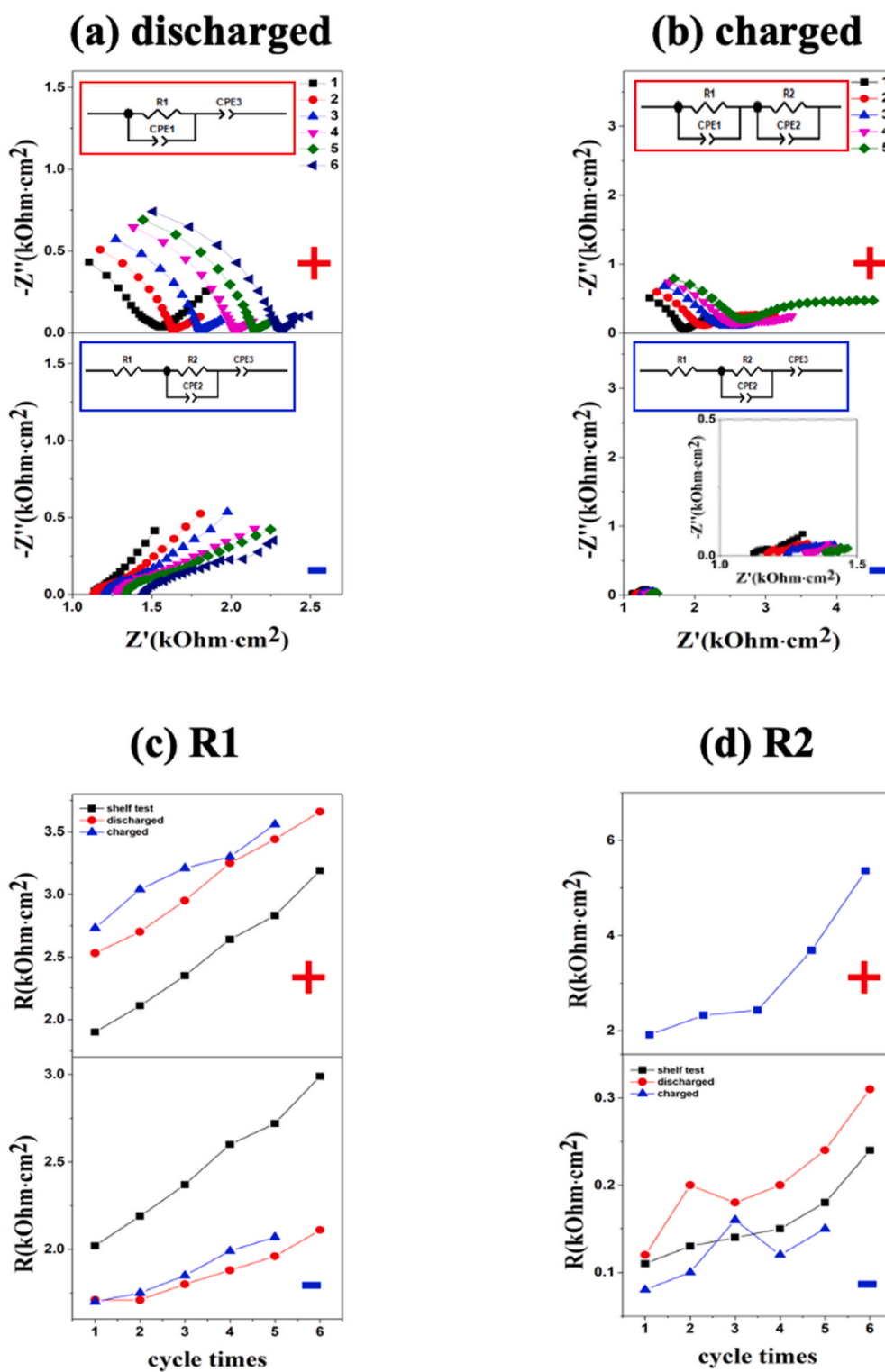


Fig. 7. (a, b) Impedance response of positive and negative electrodes in the discharged and charged states. (c, d) Fitting results of areal resistances (R1 and R2) of positive and negative electrodes in the discharged and charged states, as well as during the shelf test.

LNM was not stable with Ga-doped LLZ when being charged to 3.8 V (using Li anode), whereas our result demonstrates LNM can be stable with garnet-type solid electrolyte LLZT at a higher voltage. This is the first time to successfully apply 5 V-class LNM cathode in a battery based on garnet-type solid electrolyte. After charging, we applied the same current 0.1 C to the discharging until the whole-cell voltage dropped to 0. While the discharging voltage profile of positive-electrode (we-re)

look similar to the charging profile with a shallow sloping, the voltage of negative electrode (ce-re) increase quickly and prematurely to the cut-off voltage, such that the full discharge capacity could not be achieved. For example, the five-cycle coulombic efficiency of discharging process was 19%, 36%, 47%, 52% and 57%, respectively. The low coulombic efficiency of 1st cycle might be caused by the side reaction of  $\text{Li}_2\text{CO}_3$  or  $\text{LiOH}$  at the interface [38], and the coulombic efficiency of

following cycles kept increasing after  $\text{Li}_2\text{CO}_3$  or  $\text{LiOH}$  disappeared [42].

Impedance response results of electrolyte-cell and tri-layer cell during the shelf test are shown in Fig. 6. First, the impedance response of electrolyte-cell with silver electrodes is shown in Fig. 6(a), with a partial arc (modeled as  $\text{R1/CPE1}$  where “/” represents the parallel connection) at high frequencies and a blocking tail at lower frequencies (modeled as  $+ \text{CPE3}$  where “+” represents the series connection). As the measurement was done at  $150^\circ\text{C}$  we can ignore the grain boundary contribution and attribute the partial arc to the electrolyte based on the frequency response (i.e.  $>0.14$  MHz). In addition, the effective capacitance value of this partial arc,  $\sim 25$  pF, also suggests a bulk response. When this cell was exposed to air, the R1 resistance kept increasing based on five consecutive tests with 10-h interval, i.e. Fig. 6(a). This resistance increase is probably due to the contamination of  $\text{CO}_2$  and  $\text{H}_2\text{O}$  as reported previously [38,43].

The impedance responses of positive (i.e. we-re) and negative (i.e. ce-re) electrodes are shown in Fig. 6(b). Based on the frequency response and resistivity values of electrolyte in Fig. 6(a), equivalent circuits could be constructed to understand different processes in electrodes. For the positive-electrode, equivalent circuit was  $\text{R1/CPE1}+\text{CPE3}$ , where R1/CPE1 was the electrolyte response while CPE3 was due to diffusion in the electrode (no charge transfer processes can be separated). For the negative-electrode, equivalent circuit was  $\text{R1}+\text{R2/CPE2}+\text{CPE3}$ , corresponding to electrolyte, interface, and diffusion, respectively. Indeed, the effective capacitance of CPE2 is  $\sim \mu\text{F}$ , which suggests that it is due to the interface between solid electrolyte and electrode. The summation of R1 (i.e. electrolyte contribution) of positive and negative-electrodes is similar to the value of R1 in the electrolyte-cell as electrolytes in the two cells have similar dimensions. The 10-h interval shelf-test of the tri-layer cell also indicated that R1 and R2 of both electrodes kept increasing, to be shown in Fig. 7(c) and (d), similar to what was observed in the electrolyte cell.

Impedance response results of the tri-layer cell during the charging/discharging processes are shown in Fig. 7. Responses in the discharged state, i.e. Fig. 7(a) were similar to those during the shelf test shown in Fig. 6(b). This observation is not surprising as the fully or mostly discharged cell should have electrochemical properties similar to that in the shelf test. Therefore, the same equivalent circuits,  $\text{R1/CPE1}+\text{CPE3}$  for positive and  $\text{R1}+\text{R2/CPE2}+\text{CPE3}$  for negative, to those in the shelf test were employed for the discharged state. At the charged state, the interfacial contributions of both positive and negative electrodes can be better resolved in the impedance response (Fig. 7(b)), compared with the discharged state. While  $\text{R1}+\text{R2/CPE2}+\text{CPE3}$  is still a suitable equivalent circuit for the negative-electrode in the charged state, we applied a circuit of  $\text{R1/CPE1}+\text{R2/CPE2}$  to include the interfacial response of positive-electrode. Time evolution of R1 and R2 during cycling is shown in Fig. 7(c) and (d). As observed in the shelf test, both R1 (i.e. electrolyte) and R2 (interface) increase with cycling for both electrodes. When we compare the interfacial resistance of positive and negative-electrodes, values of negative-electrode are about 1 order of magnitude lower in the charged state, suggesting that the positive-electrode|electrolyte interface could be further improved. For example, it was reported that coating or buffer layer could mitigate this interface problem [8,11].

Examination of both the voltage profiles (Fig. 5) and impedance response (Fig. 7) of positive and negative electrodes enabled by the three-electrode analysis could offer some insights on the low coulombic efficiency observed during cycling. Although there was noticeable interfacial impedance increase for the positive electrode going from discharged (Fig. 7(a)) to charged (Fig. 7(b)), as discussed earlier, it did not change the charging/discharging voltage profile significantly, other than affecting the instantaneous voltage jump. On the other hand, although the change of interfacial impedance of the negative electrode is small, it appears that the negative electrode is the performance-limiting component in the cell. While the intercalation of LTO ( $\text{Li}_4\text{Ti}_5\text{O}_{12}$ ), Fig. 5 (a), is typical of two-phase coexistence reaction between  $\text{Li}_4\text{Ti}_5\text{O}_{12}$  and

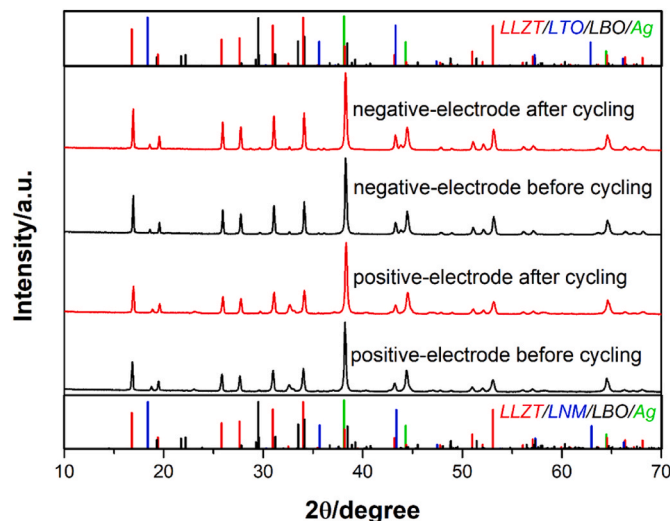


Fig. 8. Powder XRD patterns of positive and negative electrodes before and after cycling.

$\text{Li}_7\text{Ti}_5\text{O}_{12}$ , the deintercalation of  $\text{Li}_7\text{Ti}_5\text{O}_{12}$ , Fig. 5(b), seems to have larger polarization, resulting in low coulombic efficiency. This larger polarization could come from two sources: (1) deintercalation of  $\text{Li}_7\text{Ti}_5\text{O}_{12}$  is a process leading to increased interfacial impedance (going from Fig. 7(b)–a); (2) possible solid electrolyte interphase (SEI) formation between  $\text{Li}_7\text{Ti}_5\text{O}_{12}$  and LLZT due to increased Li content in the electrode. This SEI formation did not increase the interfacial impedance but induced structural change in  $\text{Li}_7\text{Ti}_5\text{O}_{12}$  in a way that slows down the phase transformation to  $\text{Li}_4\text{Ti}_5\text{O}_{12}$ . This suggests that a solid-solution, instead of a phase-coexistence, material might be a better choice for the negative electrode.

Powder XRD experiments were performed before and after cycling to check if there were significant phase evolution in the positive and negative electrode after charging/discharging. Results are shown in Fig. 8 with primary peaks attributed to LLZT electrolyte, LTO/LNM electrode, and Ag. There is negligible change in diffraction patterns before and after cycling, which suggests materials remain stable after repeated charging/discharging processes.

#### 4. Conclusions

For the first time, we showed that we could use  $\text{Li}_2\text{CO}_3$  to stabilize the interface between Ta-doped LLZ (LLZT) and LNM/LTO without producing the  $\text{La}_2\text{Zr}_2\text{O}_7$  impurity after the mixture was sintered at  $800^\circ\text{C}$ . When the electrode mixtures were supplemented with additives such as LBO and Ag, a tri-layer all-solid-state lithium-ion battery could be prepared as revealed by electron micrographs, EDS elemental mapping, and EDS line scan. The battery could be charged and discharged at 0.1 C rate for 5 cycles with charged voltages reaching as high as  $\sim 3.5$  V. The three-electrode setup employed in the present work allowed the separation of contributions of positive-electrode, negative-electrode, and electrolyte in the cell whether in the shelf test, charged or discharged state. It was found that the areal resistance of electrolyte increased with time due to exposure to air. While overall the negative electrode has lower interfacial impedance compared with the positive electrode, the charging/discharging profiles indicated that the negative electrode might be rate-limiting.

#### CRediT authorship contribution statement

**Yue Jiang:** Investigation, Methodology, Data curation, Writing – original draft. **Xiaohong Zhu:** Methodology, Supervision, Writing – review & editing, Resources, Funding acquisition. **Wei Lai:**

Methodology, Validation, Supervision, Writing – review & editing.

### Declaration of competing interest

The authors declare that they have no known competing financial interests or personal relationships that could have appeared to influence the work reported in this paper.

### Acknowledgments

This work was partially supported by the Fundamental Research Funds for Central Universities in China. Yue Jiang would like to acknowledge the financial support from the China Scholarship Council (No. 201806240110). The authors acknowledge the help of Hui Wang from the Analytical and Testing Center of Sichuan University for SEM analysis.

### Appendix A. Supplementary data

Supplementary data to this article can be found online at <https://doi.org/10.1016/j.jpowsour.2022.231278>.

### References

- J.M. Tarascon, M. Armand, Issues and challenges facing rechargeable lithium batteries, *Nature* 414 (2001) 359–367.
- J. Lu, Y. Chang, B. Song, H. Xia, J. Yang, K. Lee, L. Lu, High energy spinel-structured cathode stabilized by layered materials for advanced lithium-ion batteries, *J. Power Sources* 271 (2014) 604–613.
- J. Wolfenstine, J. Allen,  $\text{Ni}^{3+}/\text{Ni}^{2+}$  redox potential in  $\text{LiNiPO}_4$ , *J. Power Sources* 142 (2005) 389–390.
- K. Xu, Nonaqueous liquid electrolytes for lithium-based rechargeable batteries, *Chem. Rev.* 104 (2004) 4303–4417.
- S. Qin, X. Zhu, Y. Jiang, M. Ling, Z. Hu, J. Zhu, Growth of self-textured  $\text{Ga}^{3+}$ -substituted  $\text{Li}_7\text{La}_3\text{Zr}_2\text{O}_{12}$  ceramics by solid state reaction and their significant enhancement in ionic conductivity, *Appl. Phys. Lett.* 112 (2018) 113901.
- T. Thompson, S. Yu, L. Williams, R.D. Schmidt, R. Garcia-Mendez, J. Wolfenstine, J.L. Allen, E. Kioupakis, D.J. Siegel, J. Sakamoto, Electrochemical window of the Li-ion solid electrolyte  $\text{Li}_7\text{La}_3\text{Zr}_2\text{O}_{12}$ , *ACS Energy Lett.* 2 (2017) 462–468.
- V. Thangadurai, D. Pinzarú, S. Narayanan, A.K. Baral, Fast solid state Li ion conducting garnet-type structure metal oxides for energy storage, *J. Phys. Chem. Lett.* 6 (2015) 292–299.
- T. Kato, T. Hamanaka, K. Yamamoto, T. Hirayama, F. Sagane, M. Motoyama, Y. Iriyama, In-situ  $\text{Li}_7\text{La}_3\text{Zr}_2\text{O}_{12}/\text{LiCoO}_2$  interface modification for advanced all-solid-state battery, *J. Power Sources* 260 (2014) 292–298.
- X. Han, Y. Gong, K. Fu, X. He, G.T. Hitz, J. Dai, A. Pearse, B. Liu, H. Wang, G. Rublo, Y.F. Mo, V. Thangadurai, E.D. Wachsman, L. Hu, Negating interfacial impedance in garnet-based solid-state Li metal batteries, *Nat. Mater.* 16 (2017) 572–579.
- S. Ohta, T. Kobayashi, J. Seki, T. Asaoka, Electrochemical performance of an all-solid-state lithium ion battery with garnet-type oxide electrolyte, *J. Power Sources* 202 (2012) 332–335.
- F. Han, J. Yue, C. Chen, N. Zhao, X. Fan, Z. Ma, T. Gao, F. Wang, X. Guo, C. Wang, Interphase engineering enabled all-ceramic lithium battery, *Joule* 2 (2018) 497–508.
- J. Wu, W.K. Pang, V.K. Peterson, L. Wei, X. Guo, Garnet-type fast Li-ion conductors with high ionic conductivities for all-solid-state batteries, *ACS Appl. Mater. Interfaces* 9 (2017) 12461–12468.
- M. He, Z. Cui, C. Chen, Y. Li, X. Guo, Formation of self-limited, stable and conductive interfaces between garnet electrolytes and lithium anodes for reversible lithium cycling in solid-state batteries, *J. Mater. Chem. A.* 6 (2018) 11463–11470.
- G.V. Alexander, N.C. Rosero-Navarro, A. Miura, K. Tadanaga, R. Murugan, Electrochemical performance of a garnet solid electrolyte based lithium metal battery with interface modification, *J. Mater. Chem. A.* 6 (2018) 21018–21028.
- T. Liu, Y. Zhang, X. Zhang, L. Wang, S. Zhao, Y. Lin, Y. Shen, J. Luo, L. Li, C. Nan, Enhanced electrochemical performance of bulk type oxide ceramic lithium batteries enabled by interface modification, *J. Mater. Chem. A.* 6 (2018) 4649–4657.
- G. Girishkumar, B. McCloskey, A.C. Luntz, S. Swanson, W. Wilcke, Lithium-air battery: promise and challenges, *J. Phys. Chem. Lett.* 1 (2010) 2193–2203.
- R. Murugan, V. Thangadurai, W. Weppner, Fast lithium ion conduction in garnet-type  $\text{Li}_7\text{La}_3\text{Zr}_2\text{O}_{12}$ , *Angew. Chem. Int. Ed.* 46 (2007) 7778–7781.
- C. Ma, Y. Cheng, K. Yin, J. Luo, A. Sharafi, J. Sakamoto, J. Li, K.L. More, N. J. Dudney, M. Chi, Interfacial stability of Li metal–solid electrolyte elucidated via in situ electron microscopy, *Nano Lett.* 16 (2016) 7030–7036.
- D. Rettenwander, R. Wagner, A. Reyer, M. Bonta, L. Cheng, M.M. Doeff, A. Limbeck, M. Wilkening, G. Amthauer, Interface instability of Fe-stabilized  $\text{Li}_7\text{La}_3\text{Zr}_2\text{O}_{12}$  versus Li metal, *J. Phys. Chem. C* 122 (2018) 3780–3785.
- Y. Jin, P.J. McGinn, Al-doped  $\text{Li}_7\text{La}_3\text{Zr}_2\text{O}_{12}$  synthesized by a polymerized complex method, *J. Power Sources* 196 (2011) 8683–8687.
- Y. Zhu, J.G. Connell, S. Tepavcevic, P. Zapol, R. Garcia-Mendez, N.J. Taylor, J. Sakamoto, B.J. Ingram, L.A. Curtiss, J.W. Freeland, D.D. Fong, N.M. Markovic, Dopant-dependent stability of garnet solid electrolyte interfaces with lithium metal, *Adv. Energy Mater.* 9 (2019) 1803440.
- H. Koshikawa, S. Matsuda, K. Kamiya, M. Miyayama, Y. Kubo, K. Uosaki, K. Hashimoto, S. Nakanishi, Dynamic changes in charge-transfer resistance at Li metal/ $\text{Li}_7\text{La}_3\text{Zr}_2\text{O}_{12}$  interfaces during electrochemical Li dissolution/deposition cycles, *J. Power Sources* 376 (2018) 147–151.
- M.J. Wang, R. Choudhury, Jeff Sakamoto, Characterizing the Li-solid-electrolyte interface dynamics as a function of stack pressure and current density, *Joule* 3 (2019) 2165–2178.
- A.S. Aricó, P. Bruce, B. Scrosati, J.M. Tarascon, W. Schalkwijk, Nanostructured materials for advanced energy conversion and storage devices, *Nat. Mater.* 4 (2005) 366–377.
- S.W. Baek, J.M. Lee, T.Y. Kim, M.S. Song, Y. Park, Garnet related lithium ion conductor processed by spark plasma sintering for all solid state batteries, *J. Power Sources* 249 (2014) 197–206.
- R. Pfenninger, S. Afyon, I. Garbayo, M. Struzik, J.L.M. Rupp, Lithium titanate anode thin films for Li-ion solid state battery based on garnets, *Adv. Funct. Mater.* 28 (2018) 1800879.
- J. Broek, S. Afyon, J.L.M. Rupp, Interface-engineered all-solid-state Li-ion batteries based on garnet-type fast  $\text{Li}^+$  conductors, *Adv. Energy Mater.* 6 (2016) 1600736.
- J. Zhang, X. Zang, H. Wen, T. Dong, J. Chai, Y. Li, B. Chen, J. Zhao, S. Dong, J. Ma, L. Yue, Z. Liu, X. Guo, G. Cui, L. Chen, High-voltage and free-standing poly(propylene carbonate)/ $\text{Li}_{6.75}\text{La}_3\text{Zr}_{1.75}\text{Ta}_{0.25}\text{O}_{12}$  composite solid electrolyte for wide temperature range and flexible solid lithium ion battery, *J. Mater. Chem. A.* 5 (2017) 4940–4948.
- K. Yoshima, Y. Harada, N. Takami, Thin hybrid electrolyte based on garnet-type lithium-ion conductor  $\text{Li}_7\text{La}_3\text{Zr}_2\text{O}_{12}$  for 12 V-class bipolar batteries, *J. Power Sources* 302 (2016) 283–290.
- N. Takami, K. Yoshima, Yasuhiro Harada, 12 V-Class Bipolar lithium-ion batteries using  $\text{Li}_4\text{Ti}_5\text{O}_{12}$  anode for low-voltage system applications, *J. Electrochem. Soc.* 164 (1) (2017) A6254–A6259.
- H. Wang, L. Ben, H. Yu, Y. Chen, X. Yang, X. Huang, Understanding the effects of surface reconstruction on the electrochemical cycling performance of the spinel  $\text{LiNi}_{0.5}\text{Mn}_{1.5}\text{O}_4$  cathode material at elevated temperatures, *J. Mater. Chem. A.* 5 (2017) 822–834.
- S. Zhou, T. Mei, X. Wang, Y. Qian, Crystal structural design of exposed planes: express channels, high-rate capability cathodes for lithium-ion batteries, *Nanoscale* 10 (2018) 17435–17455.
- C. Hänsel, S. Afyon, J.L.M. Rupp, Investigating the all-solid-state batteries based on lithium garnets and a high potential cathode– $\text{LiMn}_{1.5}\text{Ni}_{0.5}\text{O}_4$ , *Nanoscale* 8 (2016) 18412–18420.
- Y. Yang, Y. Li, Y.Q. Li, T. Zhang, On-surface lithium donor reaction enables decarbonated lithium garnets and compatible interfaces within cathodes, *Nat. Commun.* 11 (2020) 5519.
- K. Tadanaga, R. Takano, T. Ichinose, S. Mori, A. Hayashi, M. Tatsumisago, Low temperature synthesis of highly ion conductive  $\text{Li}_7\text{La}_3\text{Zr}_2\text{O}_{12}$ - $\text{Li}_3\text{BO}_3$  composites, *Electrochem. Commun.* 33 (2013) 51–54.
- K. Park, B. Yu, J. Jung, Y. Li, W. Zhou, H. Gao, S. Son, J.B. Goodenough, Electrochemical nature of the cathode interface for a solid-state lithium-ion battery: interface between  $\text{LiCoO}_2$  and Garnet- $\text{Li}_7\text{La}_3\text{Zr}_2\text{O}_{12}$ , *Chem. Mater.* 28 (2016) 8051–8059.
- M. Tatsumisago, R. Takano, K. Tadanaga, A. Hayashi, Preparation of  $\text{Li}_3\text{BO}_3$ - $\text{Li}_2\text{SO}_4$  glass-ceramic electrolytes for all-oxide lithium batteries, *J. Power Sources* 270 (2014) 603–607.
- Y. Wang, W. Lai, Phase transition in lithium garnet oxide ionic conductors  $\text{Li}_7\text{La}_3\text{Zr}_2\text{O}_{12}$ : the role of Ta substitution and  $\text{H}_2\text{O}/\text{CO}_2$  exposure, *J. Power Sources* 275 (2015) 612–620.
- L. Miara, A. Windmuller, C.L. Tsai, W.D. Richards, Q.L. Ma, S. Uhlbruck, O. Guillon, G. Ceder, About the compatibility between high voltage spinel cathode materials and solid oxide electrolytes as a function of temperature, *ACS Appl. Mater. Interfaces* 8 (2016) 26842–26850.
- L. Guo, B. Duan, L. Zhang, Construction of controllable size silver nanoparticles immobilized on nanofibers of chitin microspheres via green pathway, *Nano Res.* 9 (7) (2016) 2149–2161.
- H. Xiang, X. Zhang, Q. Jin, C. Zhang, C. Chen, X. Ge, Effect of capacity mismatch in the  $\text{LiNi}_{0.5}\text{Mn}_{1.5}\text{O}_4/\text{Li}_4\text{Ti}_5\text{O}_{12}$  cells, *J. Power Sources* 183 (2008) 355–360.
- F. Du, N. Zhao, Y. Li, C. Chen, Z. Liu, X. Guo, All solid state lithium batteries based on lamellar garnet-type ceramic electrolytes, *J. Power Sources* 300 (2015) 24–28.
- L. Zhang, J. Yang, Y. Gao, X.P. Wang, Q.F. Fang, C.H. Chen, Influence of  $\text{Li}_3\text{BO}_3$  additives on the Li conductivity and stability of Ca/Ta-substituted  $\text{Li}_{6.55}(\text{La}_{2.95}\text{Ca}_{0.05})(\text{Zr}_{1.5}\text{Ta}_{0.5})\text{O}_{12}$  electrolytes, *J. Power Sources* 355 (2017) 69–73.